Article

Novel Flexible Triboelectric Nanogenerator based on Metallized Porous PDMS and Parylene C

Massimo Mariello [1,2,*], **Elisa Scarpa** [1], **Luciana Algieri** [3], **Francesco Guido** [1], **Vincenzo Mariano Mastronardi** [1], **Antonio Qualtieri** [1] **and Massimo De Vittorio** [1,2]

[1]   Istituto Italiano di Tecnologia, Center for Biomolecular Nanotechnologies, 73010 Arnesano (Lecce), Italy; elisa.scarpa@iit.it (E.S.); francesco.guido@iit.it (F.G.); vincenzo.mastronardi@iit.it (V.M.M.); antonio.qualtieri@iit.it (A.Q.); massimo.devittorio@iit.it (M.D.V.)
[2]   Dipartimento di Ingegneria dell'Innovazione, Università del Salento, 73100 Lecce, Italy
[3]   Piezoskin s.r.l., 73010 Arnesano (Lecce), Italy; lalgieri@piezoskin.com
[*]   Correspondence: massimo.mariello@iit.it; Tel.: +39-0832-1816-200

Abstract: Triboelectric nanogenerators (TENGs) have recently become a powerful technology for energy harvesting and self-powered sensor networks. One of their main advantages is the possibility to employ a wide range of materials, especially for fabricating inexpensive and easy-to-use devices. This paper reports the fabrication and preliminary characterization of a novel flexible triboelectric nanogenerator which could be employed for driving future low power consumption wearable devices. The proposed TENG is a single-electrode device operating in contact-separation mode for applications in low-frequency energy harvesting from intermittent tapping loads involving the human body, such as finger or hand tapping. The novelty of the device lies in the choice of materials: it is based on a combination of a polysiloxane elastomer and a poly (para-xylylene). In particular, the TENG is composed, sequentially, of a poly (dimethylsiloxane) (PDMS) substrate which was made porous and rough with a steam-curing step; then, a metallization layer with titanium and gold, deposited on the PDMS surface with an optimal substrate–electrode adhesion. Finally, the metallized structure was coated with a thin film of parylene C serving as friction layer. This material provides excellent conformability and high charge-retaining capability, playing a crucial role in the triboelectric process; it also makes the device suitable for employment in harsh, wet environments owing to its inertness and barrier properties. Preliminary performance tests were conducted by measuring the open-circuit voltage and power density under finger tapping (~2 N) at ~5 Hz. The device exhibited a peak-to-peak voltage of 1.6 V and power density peak of 2.24 mW/m^2 at ~0.4 MΩ. The proposed TENG demonstrated ease of process, simplicity, cost-effectiveness, and flexibility.

Keywords: triboelectric nanogenerator (TENG); mechanical energy harvesting; single-electrode; tapping; flexibility; porous/rough PDMS; parylene C

1. Introduction

Flexible, wearable electronics have attracted plenty of research and technology attention owing to their advantageous properties over rigid electronic systems and devices of softness, lightweight, comfort, and adaptability [1–4]. Combining these features with functional materials and specific architectures has led to the employment of flexible devices for several applications, e.g., physiological monitoring and chemical sensing [5–9], soft robotics [10–12], energy harvesting [13–17], and motion detection [18–20]. The recently increasing importance of self-powered electronics has led to the development of integrated systems with energy harvesting technologies.

However, the demand for thin, compliant, and lightweight systems for replacing batteries and supplying microelectronic devices has led to plenty of research efforts to devise efficient, miniaturized power sources. Conventional batteries, in fact, are characterized by limited capacity, necessity of periodic charging, difficulty of miniaturization, and harmfulness of employed material; thus, new energy supplying systems have been studied and proposed in recent years. Mechanical energy harvesting from ambient vibrations or friction is a very promising field and several mechanisms to convert mechanical into electrical energy (energy harvesters) have been exploited in the last years, e.g., electromagnetic [21–24], piezoelectric [25–30], and triboelectric [31–35]. Among them, the triboelectric principle is an attractive option [36]. The triboelectric effect is an electrification process induced by the contact between two different materials: the friction causes a charge separation depending on the different polarity of the materials in contact [37,38].

Triboelectric nanogenerator (TENG) was first implemented by Prof. Z. L. Wang's group in 2012 for the conversion of small-scale mechanical energy into electrical energy. Since then, this technology has spread and improved with the advent of new device architectures and the employment of new functional materials. TENG devices exhibit several advantages compared to other types of energy harvesting or sensing devices: light mass, low density and cost, they are not based on magnets or coils like classical electromagnetic generators, and they exhibit their best performances at low frequencies (<10 Hz). Thus, they are suitable for applications regarding human body motion and ocean waves [31,37,39–41].

TENG technology exploits four main basic operation modes, as previously reported in [37]: (i) vertical contact-separation mode; (ii) lateral sliding mode; (iii) single-electrode mode; (iv) freestanding triboelectric-layer mode. Although the single-electrode devices exhibit lower ranges of generated voltages and powers [42], they are generally characterized by simpler architectures, ease of process, and suitability of energy generation by intermittent tapping onto the device. For these reasons, they are suitable for applications involving the human body, such as finger and hand tapping or walking on the floor [37,43].

Many examples of triboelectric energy harvesters have been proposed worldwide, with different operation modes [31,33,39,44–50]. In this respect, the search and exploitation of new friction materials is ongoing [32,36,39,51–53], as well as new techniques for enhancing triboelectric charge transfer based on surface treatments, nanostructured patterns, or modifications of roughness and porosity [43,52,54,55].

Zhang et al. [56] demonstrated a flexible single-electrode TENG based on double-sided PDMS surface nanostructures (nanopillars with diameter of about 200 nm, made by imprint lithography): the device has good output performance at low frequencies, up to 160 V, 3 μA, and 423.8 mW/m^2 for the open-circuit voltage, short-circuit current, and power density, respectively, under applied pressure forces in the range of 0.5–50 N.

Nguyen et al. [57] showed the possibility to enhance the output performances of a peptide-based piezoelectric nanogenerator by utilizing a single-electrode TENG without additional conductive electrodes based on the vertical contact-separation of two triboelectric materials, kapton and poly (ethyleneterephtalate) (PET). The open-circuit voltage and short-circuit current of the triboelectric component under an applied force of 50 N are about 1.6 V and 20 nA, respectively, which can be superimposed to the outputs of the piezoelectric part, 0.7 V and 30 nA, respectively.

Wang et al. [58] reported the fabrication of a single-electrode TENG based on sponge-like porous poly (tetrafluoroethylene) (PTFE) thin films made by using deionized water as soft template. In this case, porosity contributes to enhancing the output performances by a factor of 1.8 on the generated voltage compared to the non-porous control; an output voltage of 1.1 V can be achieved by pressing the device with a bare human hand.

The need and demand for simple fabrication techniques for TENGs is ongoing, and major efforts for developing or employing flexible cost-effective materials are still required.

This paper reports on the low-cost fabrication of a novel flexible single-electrode TENG operating in contact-separation mode based on metallized porous PDMS and parylene C (pC). The novelty of

the device lies in the choice of materials: the porosity of metallized PDMS and the charge-retaining capability of pC play a crucial role in the triboelectric working mechanism.

Parylene C was chosen as friction layer by virtue of its desirable outstanding properties of optimal conformality, chemical inertness, and compactness: it is an excellent coating for different types of substrates and the synthesis process is very efficient in allowing complete control of the deposition parameters [59]. Parylene is used as a protective coating for biomedical devices and microelectronics [60], but it also reveals great potential as a charge accumulation layer during the triboelectrification process because surface charge densities higher than 2.0 mC/m^2 may be achieved [54,61].

2. Materials and Methods

2.1. Materials

Silicon wafers or glass slides were used as substrates for the deposition of PDMS by spin-coating.

PDMS (Sylgard 184 Silicone Elastomer) was supplied by Dow Corning Corporation in two forms: a viscous uncured pre-polymer and a curing agent. Parylene C was provided by Specialty Coating Systems in form of dimer powders. Kapton HN 25 μm-thick foils were supplied by DuPont.

2.2. Fabrication of Flexible TENG

In Figure 1A,B a schematic representation and captured images of the fabricated devices are reported, showing an active area of the device of 2×2 cm^2, while Figure 1C illustrates the steps of the fabrication process.

After curing (100 °C, 10 min) a 160 μm-thick spin-coated PDMS film (Figure 1C(i)), and a thinner PDMS layer (15–20 μm) were deposited at a higher spinning speed (2000 rpm) and cured with water vapor (100 °C) for 5 min (Figure 1C(ii)).

A flask filled with distilled water was placed on a hot plate (at 120 °C) and connected through a temperature-resistant rubber tube to a glass chamber containing the samples (see Figure 2A). The tube inlet was controlled by a valve which was opened when the water inside the flasks reached a constant temperature and pressure. The tube outlet was enlarged with a glass funnel in order to achieve a wide vapor jet. The steam-curing step, as previously described in [62], was adopted to produce asperities and pores which allow the adhesion of metal layers onto PDMS and favor the charge generation during contact of friction layers in the triboelectric device. The residual water droplets that condensed on the PDMS surface were removed under a nitrogen flow and by heating the sample (120 °C, 10 min).

The metal electrodes of the devices were made by metallizing the PDMS substrate by physical vapor deposition processes: titanium (50 nm) was first deposited as adhesion promoter (Figure 1C(iii)) by reactive sputtering and then gold (50 nm) was thermally evaporated as exposed electrode (Figure 1C(iv)]. After peeling off the flexible patch (Figure 1C(v)), it was attached onto a 25 μm-thick kapton foil and used as support for the connections (Figure 1C(vi)): an electrical wire was connected using a rivet and a ~2.5 μm-thick parylene C film was then deposited by room temperature chemical vapor deposition (RT-CVD) step (Figure 1C(vii)).
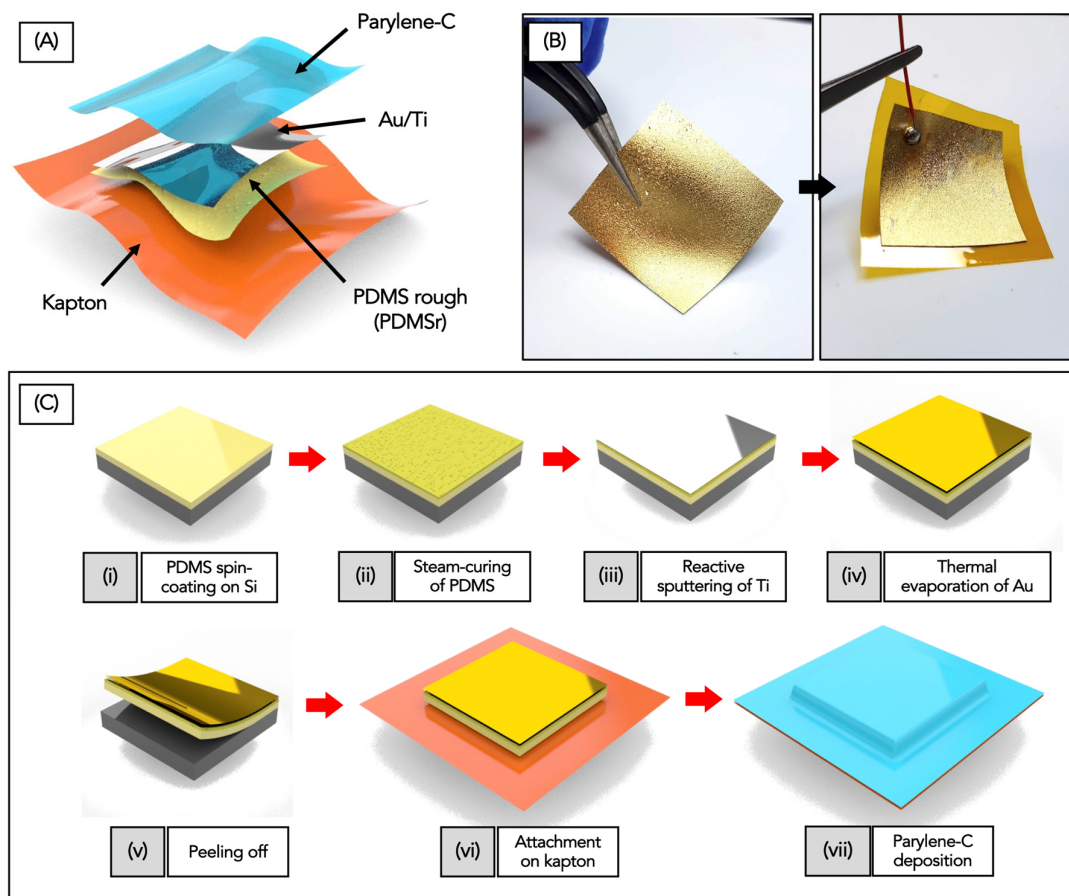
Figure 1. Schematic representation (**A**) and photos (**B**) of the triboelectric nanogenerator with the indication of the constituent layers. (**C**) Fabrication process of the proposed triboelectric nanogenerator: (i) PDMS spin-coating on Si wafer; (ii) Steam-curing of PDMS; (iii) Reactive sputtering of Ti; (iv) Thermal evaporation of Au; (v) Peeling off of the metallized patch; (vi) Attachment of the patch on a kapton foil; (vii) Parylene C conformal deposition.

2.3. Characterization of Flexible TENG

The morphology of the metallized flat patches were analyzed by means of a profilometer (Bruker Dektak Xt) and atomic force microscopy (AFM), and the surface porosity was observed with an optical microscope (Nikon Eclipse L200NSD Microscope) and by scanning electron microscopy (SEM, Helios NanoLab 600i, FEI). The electrical resistance of the flexible substrates were measured with a multimeter: the probes were positioned on the metal side of the metallized porous PDMS patches before pC deposition. Preliminary output generation tests were performed under finger tapping by connecting the device to an oscilloscope (Tektronix MDO 4104-3) and to a source meter (Keithley Series 2400), for measuring the open-circuit voltage and the short-circuit current. The power curve of the device was obtained by measuring the voltage drop on a variable resistive load connected to the device. Mechanical tensile tests were conducted by dynamic mechanical analysis (DMA Q800 TA Instruments).
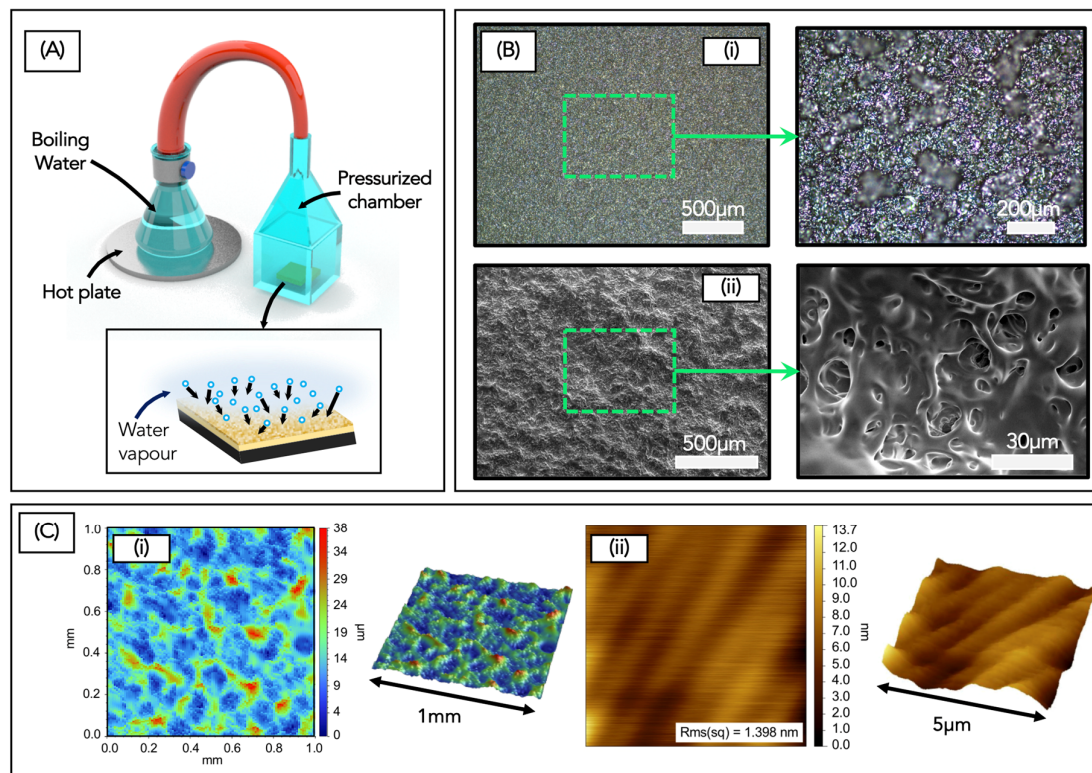
Figure 2. (**A**) Setup used for the steam-curing step to make the PDMS patch rough and porous in the superficial layer; the inset shows the impingement of water vapor particles onto the PDMS surface. (**B**) Optical micrographs (i) and SEM micrographs (ii) showing the morphology of the rough PDMS layer. (**C**) 2D and 3D topography images of the rough PDMS layer, scanned with the profilometer (i) and by AFM (ii), on 1 mm^2 and 5 μm^2 areas, respectively.

3. Results and Discussion

This study shows the low-cost fabrication of a novel flexible single-electrode TENG operating in contact-separation mode and based on metallized porous PDMS and parylene C (pC).

The parylene film acts as friction layer, while the PDMS patch confers flexibility and adaptability, making the device suitable for smart clothes and wearable technology.

The optical and SEM micrographs in Figure 2B(i,ii) show the surface morphology of the flat metallized PDMS patches: it can be observed that the steam-curing step produced a regular porosity and the pore diameters are in the range of 5–30 μm.

The topography images (see Figure 2C(i)), taken with the profilometer, provide information about the height of asperities produced by the water vapor on scanned areas of 1×1 mm^2: a maximum roughness of 30–40 μm was measured, as shown by the colored bar. A lower-range morphology, at the inner surface of the pores, was observed with AFM, as reported by the micrographs in Figure 2C(ii): the roughness (Rms(sq)) of a scanned area of 5×5 μm^2 was 1.398 nm.

The electrical resistance of the flat metallized PDMS patch (~2×2 cm^2) was ~3 Ω/sq and it was measured for different bending angles (as defined in the inset) and stretching ratios to test its flexibility (see Figure 3A,B respectively). It increases with decreasing bending angles and with increasing stretching ratios, since the micropores get wider, reducing the number of conductive pathways in the metal layers. However, the electrical resistance of unbent/unstretched substrate is recovered because of the strong adhesion between the Ti/Au metallization and the porous PDMS. Thus, the surface porosity induced by the steam-curing step contributes not only for the triboelectrification process, but primarily for allowing the adhesion of the metal layers onto the soft PDMS substrate.
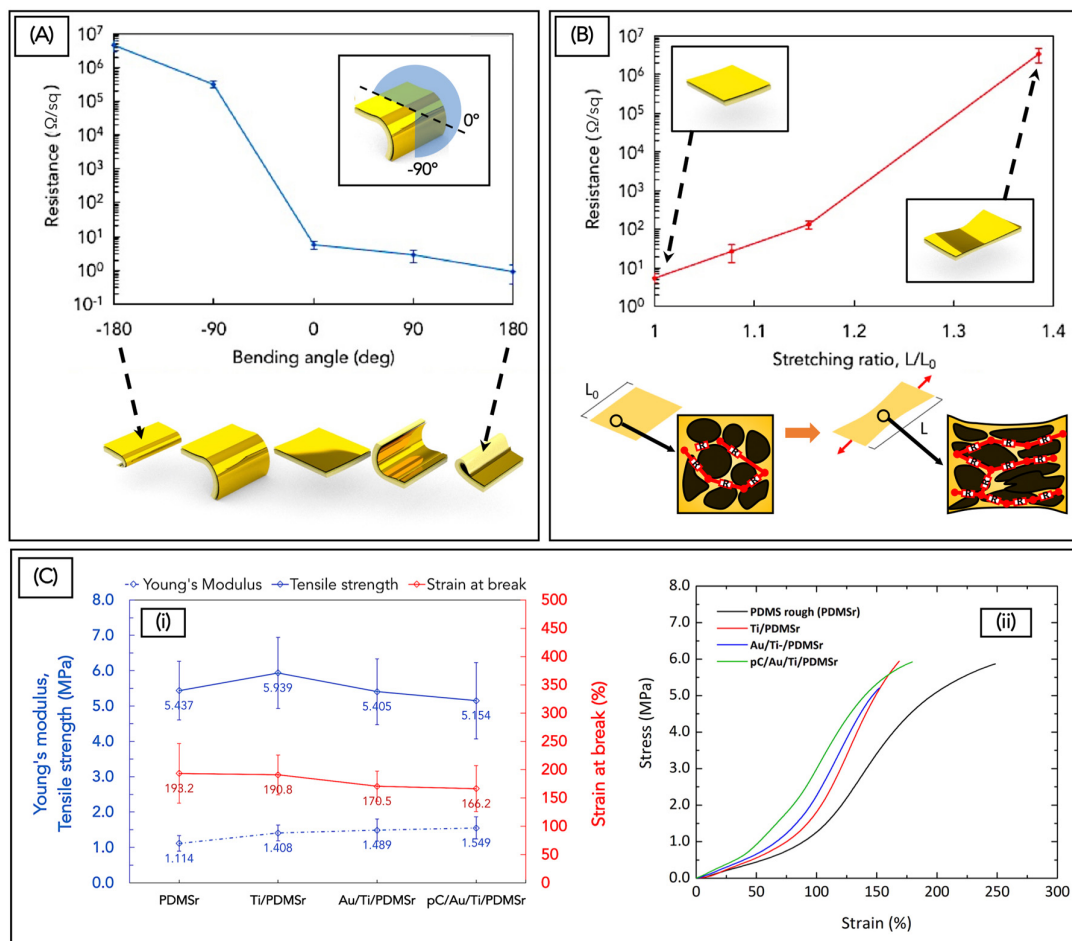
Figure 3. (**A**) Measurement of electrical resistance of the metallized PDMS patch as a function of the bending angle. (**B**) Measurement of electrical resistance of the metallized PDMS patch as a function of the stretching ratio; the insets show the conductive pathways inside the porous morphology of the patch. (**C**) Dynamic mechanical analysis (DMA) of the PDMS rough patch with the overlying layers. (i) Summary plot of the Young's modulus, tensile strength, and strain at break of neat rough PDMS (PDMSr) and covered with Ti, Au/Ti, and pC/Au/Ti. (ii) Stress–strain curves obtained after the tensile tests of the same samples.

Stress–strain curves obtained by dynamic mechanical analysis are reported in Figure 3C(ii) for the rough PDMS patch (PDMSr) and the patches metallized with Ti, Au/Ti, and covered with a parylene layer. The Young's modulus, tensile strength, and strain at break of the samples were deduced from the curves for each sample and summarized in Figure 3C(i): the range for the measured quantities is comparable for the differently metallized patches and a slight increase in the Young's modulus can be observed, due to the deposition of metal and parylene films onto the PDMS patch. The PDMS-based triboelectric device without the kapton support exhibits a Young's modulus of 1.549 MPa, a tensile strength of 5.154 MPa, and a strain at break of 166.2%.

The presented TENG was fabricated as single-electrode device for energy harvesting from a low-frequency source, in particular, from human body motion. Performance preliminary tests were thus conducted by measuring the open-circuit voltage under finger tapping. The average applied force and frequency of the load were measured with a force resistive sensor (FSR 402, Interlink Electronics Sensor Technologies), resulting as ~2 N and ~5 Hz. The output voltage was measured with the oscilloscope for different parylene (pC) thicknesses: as illustrated by the plot in Figure 4C, the voltage decreases with increasing pC thickness, mainly due to the decrease in the capacity of the triboelectric device as well as the higher rigidity of the layered structure. In particular, the device

exhibited a peak-to-peak voltage of ~1.6 V for 1 μm-thick pC, and up to ~0.6 V for 6 μm-thick pC. Consequently, the generation tests were performed by choosing a pC thickness of 1 μm: the maximum peak-to-peak open-circuit voltage and short-circuit current, measured with oscilloscope and source meter respectively, were ~1.6 V and ~0.15 μA (Figure 4A,B). The power density curve is reported in Figure 4D, as calculated after measuring the average peak-to-peak voltage drop on the resistive loads connected to the TENG, according to the following expression:

$$p = \frac{\langle P \rangle}{S} = \frac{V^2/R_{\Omega}}{S} \tag{1}$$

where p is the output power density (mW/m^2) $\langle P \rangle$ is the output power (mW); S is the TENG active area (m^2); R_{Ω}, V are the resistance (Ω) and the peak-to-peak voltage drop (V) on the resistive load, respectively. The maximum power is reached when the device is closed on an optimal load matching the device electrical impedance [63]: the peak of power density was 2.24 mW/m^2 at ~0.4 MΩ (Figure 4D).
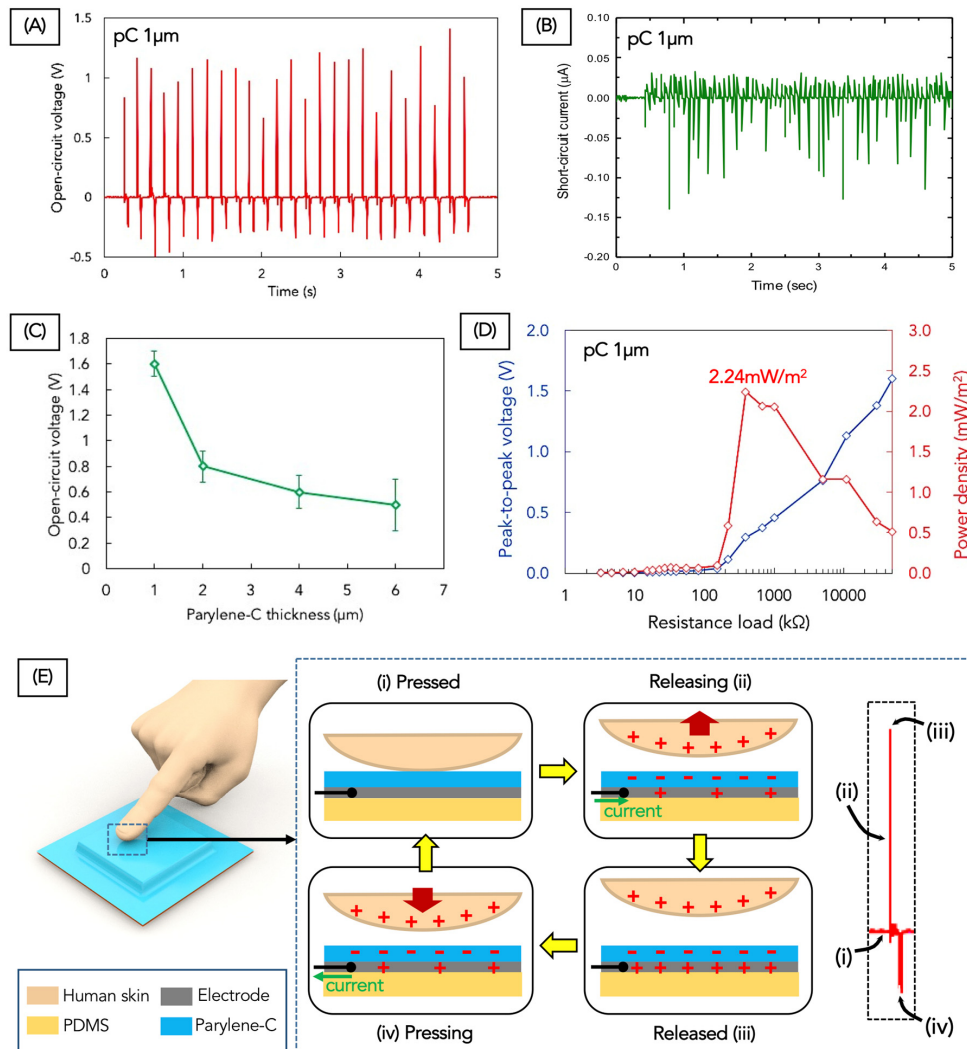
Figure 4. Open-circuit voltage (**A**) and short-circuit current (**B**) generated by the proposed triboelectric nanogenerator (TENG) with the triboelectric parylene C layer of 1 μm, under finger tapping of ~2N at ~5Hz. (**C**) Open-circuit voltage as a function of the parylene C thickness. (**D**) Peak-to-peak voltage and power density generated by the TENG with parylene C thickness of 1 μm as a function of the resistive load. (**E**) Proposed working principle for the TENG under finger tapping: the steps of the press–release cycle are illustrated and indicated for the inset of the output voltage signal.

In Figure 4E, the proposed working mechanism of the TENG is illustrated. The exact operation mode is defined as conductor-to-dielectric single-electrode vertical contact-separation TENG, and the conductor approaching the device is represented by the naked finger. At the initial state of the press–release cycle (Figure 4E(i)), the finger and the upper layer of parylene C are brought into contact, such that surface charge transfer takes place due to the friction and contact electrification effect. According to the triboelectric series, human dry skin acts as a positive tribo-material [42,64,65] so positive charges are generated on the skin surface and the same amount of negative charges form on the surface of parylene coating according to the charge conservation principle. Therefore, positive charges are electrostatically induced on the primary electrode underneath parylene (Ti/Au metallization). The triboelectric charges on parylene are confined on the surface because it is an insulator, so during contact (Figure 4E(i)), charges with opposite signs reside almost on the same plane, and no electrical potential difference is established between the two sides. When the finger starts to separate from the parylene surface (Figure 4E(ii)), a potential difference arises between the primary electrode and the ground under open-circuit conditions, increasing with the vertical finger–parylene separation distance (up to 1–2 cm for complete release in Figure 4E(iii)). In short-circuit conditions, the voltage drop drives an electron transfer, thus generating an instantaneous current from the ground to the electrode, forcing them to have the same potential. A successive approach of the finger to parylene (Figure 4E(iv)) triggers the same mechanisms, but in the opposite way, because the potential difference decreases and the electrons are driven from the primary electrode to the ground.

The TENG proposed in the present work is envisioned to be easily employed in distributed arrays to meet the power requirements of various wearable, flexible energy harvesting devices. Moreover, the adoption of parylene C as an external encapsulating friction layer makes the device suitable for employment in harsh environments; for instance, for scavenging energy from falling raindrops, since the protective anti-corrosion and anti-biofouling behavior of parylene have been demonstrated in previous works [60,66–69].

4. Conclusions

Our research shows an easy fabrication method for a flexible contact-separation mode triboelectric nanogenerator (TENG) based on novel combinations of materials, in essence, a porous PDMS substrate metallized with titanium and gold and coated with a conformal thin film of parylene C.

The TENG is a single-electrode device, so it is characterized by simpler architecture and ease of process if compared to more complex operation modes. It is particularly suitable for energy generation by intermittent tapping onto the device and, thus, for applications involving the human body such as finger and hand tapping or walking on the floor.

Performance preliminary tests were conducted by measuring the open-circuit voltage and power density under finger tapping (~2 N) at ~5 Hz. The device exhibited a peak-to-peak voltage of ~1.6 V and the peak of power density was 2.24 mW/m^2 at ~0.4 MΩ. The working mechanism of the TENG was proposed for contact with human skin based on the experimental results. The use of parylene C lets us envision the possibility to employ the device in harsh environments, where humidity or other aggressive agents are present.

References

1. Chen, H.; Song, Y.; Guo, H.; Miao, L.; Chen, X.; Su, Z.; Zhang, H. Hybrid porous micro structured finger skin inspired self-powered electronic skin system for pressure sensing and sliding detection. *Nano Energy* **2018**, *51*, 496–503. [CrossRef]

2. Wang, S.; Xu, J.; Wang, W.; Wang, G.-J.N.; Rastak, R.; Molina-Lopez, F.; Chung, J.W.; Niu, S.; Feig, V.R.; Lopez, J.; et al. Skin electronics from scalable fabrication of an intrinsically stretchable transistor array. *Nature* **2018**, *555*, 83–88. [CrossRef] [PubMed]

3. Chortos, A.; Liu, J.; Bao, Z. Pursuing prosthetic electronic skin. *Nat. Mater.* **2016**, *15*, 937–950. [CrossRef] [PubMed]

4. Gu, Y.; Zhang, T.; Chen, H.; Wang, F.; Pu, Y.; Gao, C.; Li, S. Mini Review on Flexible and Wearable Electronics for Monitoring Human Health Information. *Nanoscale Res. Lett.* **2019**, *14*, 263. [CrossRef] [PubMed]

5. Wang, C.; Li, X.; Hu, H.; Zhang, L.; Huang, Z.; Lin, M.; Zhang, Z.; Yin, Z.; Huang, B.; Gong, H.; et al. Monitoring of the central blood pressure waveform via a conformal ultrasonic device. *Nat. Biomed. Eng.* **2018**, *2*, 687–695. [CrossRef]

6. Gao, W.; Emaminejad, S.; Nyein, H.Y.Y.; Challa, S.; Chen, K.; Peck, A.; Fahad, H.M.; Ota, H.; Shiraki, H.; Kiriya, D.; et al. Fully integrated wearable sensor arrays for multiplexed in situ perspiration analysis. *Nature* **2016**, *529*, 509–514. [CrossRef]

7. Chung, M.; Fortunato, G.; Radacsi, N. Wearable flexible sweat sensors for healthcare monitoring: A review. *J. R. Soc. Interface* **2019**, *16*, 20190217. [CrossRef]

8. Tee, B.C.-K.; Chortos, A.; Berndt, A.; Nguyen, A.K.; Tom, A.; McGuire, A.; Lin, Z.C.; Tien, K.; Bae, W.-G.; Wang, H.; et al. A skin-inspired organic digital mechanoreceptor. *Science* **2015**, *350*, 313–316. [CrossRef]

9. Jang, K.-I.; Li, K.; Chung, H.U.; Xu, S.; Jung, H.N.; Yang, Y.; Kwak, J.W.; Jung, H.H.; Song, J.; Yang, C.; et al. Self-assembled three dimensional network designs for soft electronics. *Nat. Commun.* **2017**, *8*, 15894. [CrossRef]

10. Byun, J.; Lee, Y.; Yoon, J.; Lee, B.; Oh, E.; Chung, S.; Lee, T.; Cho, K.-J.; Kim, J.; Hong, Y. Electronic skins for soft, compact, reversible assembly of wirelessly activated fully soft robots. *Sci. Robot.* **2018**, *3*. [CrossRef]

11. Lai, Y.-C.; Deng, J.; Liu, R.; Hsiao, Y.-C.; Zhang, S.L.; Peng, W.; Wu, H.-M.; Wang, X.; Wang, Z.L. Actively Perceiving and Responsive Soft Robots Enabled by Self-Powered, Highly Extensible, and Highly Sensitive Triboelectric Proximity- and Pressure-Sensing Skins. *Adv. Mater.* **2018**, *30*, e1801114. [CrossRef] [PubMed]

12. Ju, H.; Jeong, J.; Kwak, P.; Kwon, M.; Lee, J. Robotic Flexible Electronics with Self-Bendable Films. *Soft Robot.* **2018**, *5*, 710–717. [CrossRef] [PubMed]

13. Park, S.; Heo, S.W.; Lee, W.; Inoue, D.; Jiang, Z.; Yu, K.; Jinno, H.; Hashizume, D.; Sekino, M.; Yokota, T.; et al. Self-powered ultra-flexible electronics via nano-grating-patterned organic photovoltaics. *Nature* **2018**, *561*, 516–521. [CrossRef] [PubMed]

14. Chen, J.; Huang, Y.; Zhang, N.; Zou, H.; Liu, R.; Tao, C.; Fan, X.; Wang, Z.L. Micro-cable structured textile for simultaneously harvesting solar and mechanical energy. *Nat. Energy* **2016**, *1*, 16138. [CrossRef]

15. Kim, S.J.; Lee, H.E.; Choi, H.; Kim, Y.; We, J.H.; Shin, J.S.; Lee, K.J.; Cho, B.J. High-Performance Flexible Thermoelectric Power Generator Using Laser Multiscanning Lift-Off Process. *ACS Nano* **2016**, *10*, 10851–10857. [CrossRef]

16. García Núñez, C.; Manjakkal, L.; Dahiya, R. Energy autonomous electronic skin. *Npj Flex. Electron.* **2019**, *3*, 1–24. [CrossRef]

17. Dagdeviren, C.; Yang, B.D.; Su, Y.; Tran, P.L.; Joe, P.; Anderson, E.; Xia, J.; Doraiswamy, V.; Dehdashti, B.; Feng, X.; et al. Conformal piezoelectric energy harvesting and storage from motions of the heart, lung, and diaphragm. *Proc. Natl. Acad. Sci. USA* **2014**, *111*, 1927–1932. [CrossRef]

18. Lee, S.; Reuveny, A.; Reeder, J.; Lee, S.; Jin, H.; Liu, Q.; Yokota, T.; Sekitani, T.; Isoyama, T.; Abe, Y.; et al. A transparent bending-insensitive pressure sensor. *Nat. Nanotechnol.* **2016**, *11*, 472–478. [CrossRef]

19. Guo, S.-Z.; Qiu, K.; Meng, F.; Park, S.H.; McAlpine, M.C. 3D Printed Stretchable Tactile Sensors. *Adv. Mater.* **2017**, *29*, 1701218. [CrossRef]

20. Liu, C.; Huang, N.; Xu, F.; Tong, J.; Chen, Z.; Gui, X.; Fu, Y.; Lao, C. 3D Printing Technologies for Flexible Tactile Sensors toward Wearable Electronics and Electronic Skin. *Polymers* **2018**, *10*, 629. [CrossRef]

21. Liu, H.; Hou, C.; Lin, J.; Li, Y.; Shi, Q.; Chen, T.; Sun, L.; Lee, C. A non-resonant rotational electromagnetic energy harvester for low-frequency and irregular human motion. *Appl. Phys. Lett.* **2018**, *113*, 203901. [CrossRef]

22. Liu, S.; Li, P.; Yang, Y. On the design of an electromagnetic aeroelastic energy harvester from nonlinear flutter. *Meccanica* **2018**, *53*, 2807–2831. [CrossRef]

23. Sardini, E.; Serpelloni, M. Nonlinear electromagnetic generators with polymeric materials for power harvesting from vibrations. *Procedia Eng.* **2010**, *5*, 1168–1171. [CrossRef]

24. Wang, D.-A.; Chiu, C.-Y.; Pham, H.-T. Electromagnetic energy harvesting from vibrations induced by Kármán vortex street. *Mechatronics* **2012**, *22*, 746–756. [CrossRef]

25. Akaydin, H.D.; Elvin, N.; Andreopoulos, Y. Energy Harvesting from Highly Unsteady Fluid Flows using Piezoelectric Materials. *J. Intell. Mater. Syst. Struct.* **2010**, *21*, 1263–1278. [CrossRef]

26. Dagdeviren, C.; Joe, P.; Tuzman, O.L.; Park, K.-I.; Lee, K.J.; Shi, Y.; Huang, Y.; Rogers, J.A. Recent progress in flexible and stretchable piezoelectric devices for mechanical energy harvesting, sensing and actuation. *Extreme Mech. Lett.* **2016**, *9*, 269–281. [CrossRef]

27. Hobeck, J.; Inman, D. Artificial piezoelectric grass for energy harvesting from turbulence-induced vibration. *Smart Mater. Struct.* **2012**, *21*, 105024. [CrossRef]

28. Fan, K.; Liu, Z.; Liu, H.; Wang, L.; Zhu, Y.; Yu, B. Scavenging energy from human walking through a shoe-mounted piezoelectric harvester. *Appl. Phys. Lett.* **2017**, *110*, 143902. [CrossRef]

29. Wong, V.-K.; Ho, J.-H.; Chai, A.-B. Performance of a piezoelectric energy harvester in actual rain. *Energy* **2017**, *124*, 364–371. [CrossRef]

30. Petrini, F.; Gkoumas, K. Piezoelectric energy harvesting from vortex shedding and galloping induced vibrations inside HVAC ducts. *Energy Build.* **2018**, *158*, 371–383. [CrossRef]

31. Khan, U.; Kim, S.-W. Triboelectric Nanogenerators for Blue Energy Harvesting. *ACS Nano* **2016**, *10*, 6429–6432. [CrossRef] [PubMed]

32. Choi, A.Y.; Lee, C.J.; Park, J.; Kim, D.; Kim, Y.T. Corrugated Textile based Triboelectric Generator for Wearable Energy Harvesting. *Sci. Rep.* **2017**, *7*, 45583. [CrossRef] [PubMed]

33. Hou, T.-C.; Yang, Y.; Zhang, H.; Chen, J.; Chen, L.-J.; Lin Wang, Z. Triboelectric nanogenerator built inside shoe insole for harvesting walking energy. *Nano Energy* **2013**, *2*, 856–862. [CrossRef]

34. Kim, D.Y.; Kim, H.S.; Kong, D.S.; Choi, M.; Kim, H.B.; Lee, J.-H.; Murillo, G.; Lee, M.; Kim, S.S.; Jung, J.H. Floating buoy-based triboelectric nanogenerator for an effective vibrational energy harvesting from irregular and random water waves in wild sea. *Nano Energy* **2018**, *45*, 247–254. [CrossRef]

35. Pu, X.; Liu, M.; Chen, X.; Sun, J.; Du, C.; Zhang, Y.; Zhai, J.; Hu, W.; Wang, Z.L. Ultrastretchable, transparent triboelectric nanogenerator as electronic skin for biomechanical energy harvesting and tactile sensing. *Sci. Adv.* **2017**, *3*, e1700015. [CrossRef] [PubMed]

36. Fan, F.-R.; Tian, Z.-Q.; Lin Wang, Z. Flexible triboelectric generator. *Nano Energy* **2012**, *1*, 328–334. [CrossRef]

37. Wang, Z.; Lin, L.; Chen, J.; Niu, S.; Zi, Y. *Triboelectric Nanogenerators*; Green Energy and Technology; Springer International Publishing: Berlin/Heidelberg, Germany, 2016; ISBN 978-3-319-40038-9.

38. Henniker, J. Triboelectricity in Polymers. *Nature* **1962**, *196*, 474. [CrossRef]

39. Chen, J.; Yang, J.; Li, Z.; Fan, X.; Zi, Y.; Jing, Q.; Guo, H.; Wen, Z.; Pradel, K.C.; Niu, S.; et al. Networks of Triboelectric Nanogenerators for Harvesting Water Wave Energy: A Potential Approach toward Blue Energy. *ACS Nano* **2015**, *9*, 3324–3331. [CrossRef]

40. Jiang, T.; Zhang, L.M.; Chen, X.; Han, C.B.; Tang, W.; Zhang, C.; Xu, L.; Wang, Z.L. Structural Optimization of Triboelectric Nanogenerator for Harvesting Water Wave Energy. *ACS Nano* **2015**, *9*, 12562–12572. [CrossRef]

41. Mariello, M.; Guido, F.; Mastronardi, V.M.; Todaro, M.T.; Desmaële, D.; De Vittorio, M. Nanogenerators for harvesting mechanical energy conveyed by liquids. *Nano Energy* **2019**, *57*, 141–156. [CrossRef]

42. Zi, Y.; Niu, S.; Wang, J.; Wen, Z.; Tang, W.; Wang, Z.L. Standards and figure-of-merits for quantifying the performance of triboelectric nanogenerators. *Nat. Commun.* **2015**, *6*, 8376. [CrossRef] [PubMed]

43. Niu, S.; Liu, Y.; Wang, S.; Lin, L.; Zhou, Y.S.; Hu, Y.; Wang, Z.L. Theoretical Investigation and Structural Optimization of Single-Electrode Triboelectric Nanogenerators. *Adv. Funct. Mater.* **2014**, *24*, 3332–3340. [CrossRef]

44. Phan, H.; Shin, D.-M.; Heon Jeon, S.; Young Kang, T.; Han, P.; Han Kim, G.; Kook Kim, H.; Kim, K.; Hwang, Y.-H.; Won Hong, S. Aerodynamic and aeroelastic flutters driven triboelectric nanogenerators for harvesting broadband airflow energy. *Nano Energy* **2017**, *33*, 476–484. [CrossRef]

45. Zhang, L.; Zhang, B.; Chen, J.; Jin, L.; Deng, W.; Tang, J.; Zhang, H.; Pan, H.; Zhu, M.; Yang, W.; et al. Lawn Structured Triboelectric Nanogenerators for Scavenging Sweeping Wind Energy on Rooftops. *Adv. Mater.* **2016**, *28*, 1650–1656. [CrossRef]

46. Chen, X.; He, J.; Song, L.; Zhang, Z.; Tian, Z.; Wen, T.; Zhai, C.; Chen, Y.; Cho, J.; Chou, X.; et al. Flexible one-structure arched triboelectric nanogenerator based on common electrode for high efficiency energy harvesting and self-powered motion sensing. *AIP Adv.* **2018**, *8*, 45022. [CrossRef]

47. Pu, X.; Guo, H.; Chen, J.; Wang, X.; Xi, Y.; Hu, C.; Wang, Z. Eye motion triggered self-powered mechnosensational communication system using triboelectric nanogenerator. *Sci. Adv.* **2017**, *3*, e1700694. [CrossRef]

48. Chen, B.D.; Tang, W.; He, C.; Deng, C.R.; Yang, L.J.; Zhu, L.P.; Chen, J.; Shao, J.J.; Liu, L.; Wang, Z.L. Water wave energy harvesting and self-powered liquid-surface fluctuation sensing based on bionic-jellyfish triboelectric nanogenerator. *Mater. Today* **2018**, *21*, 88–97. [CrossRef]

49. Quan, Z.; Han, C.B.; Jiang, T.; Wang, Z.L. Robust Thin Films-Based Triboelectric Nanogenerator Arrays for Harvesting Bidirectional Wind Energy. *Adv. Energy Mater.* **2016**, *6*, 1501799. [CrossRef]

50. Lin, Z.-H.; Cheng, G.; Li, X.; Yang, P.-K.; Wen, X.; Lin Wang, Z. A multi-layered interdigitative-electrodes-based triboelectric nanogenerator for harvesting hydropower. *Nano Energy* **2015**, *15*, 256–265. [CrossRef]

51. Wen, R.; Guo, J.; Yu, A.; Zhang, K.; Kou, J.; Zhu, Y.; Zhang, Y.; Li, B.-W.; Zhai, J. Remarkably enhanced triboelectric nanogenerator based on flexible and transparent monolayer titania nanocomposite. *Nano Energy* **2018**, *50*, 140–147. [CrossRef]

52. Arcot Narasimulu, A.; Zhao, P.; Soin, N.; Kovur, P.; Ding, P.; Chen, J.; Dong, S.; Chen, L.; Zhou, E.; Montemagno, C.; et al. Significant triboelectric enhancement using interfacial piezoelectric ZnO nanosheet layer. *Nano Energy* **2017**, *40*, 471–480. [CrossRef]

53. Kil Yun, B.; Soo Kim, H.; Joon Ko, Y.; Murillo, G.; Hoon Jung, J. Interdigital electrode based triboelectric nanogenerator for effective energy harvesting from water. *Nano Energy* **2017**, *36*, 233–240. [CrossRef]

54. Ravichandran, A.N.; Ramuz, M.; Blayac, S. Increasing surface charge density by effective charge accumulation layer inclusion for high-performance triboelectric nanogenerators. *MRS Commun.* **2019**, *9*, 682–689. [CrossRef]

55. Kim, H.-J.; Yim, E.-C.; Kim, J.-H.; Kim, S.-J.; Park, J.-Y.; Oh, I.-K. Bacterial Nano-Cellulose Triboelectric Nanogenerator. *Nano Energy* **2017**, *33*, 130–137. [CrossRef]

56. Zhang, M.; Xia, L.; Dang, S.; Shi, L.; Cao, A.; Deng, Q.; Du, C. A flexible single-electrode-based triboelectric nanogenerator based on double-sided nanostructures. *AIP Adv.* **2019**, *9*, 75221. [CrossRef]

57. Nguyen, V.; Kelly, S.; Yang, R. Piezoelectric peptide-based nanogenerator enhanced by single-electrode triboelectric nanogenerator. *APL Mater.* **2017**, *5*, 74108. [CrossRef]

58. Wang, M.; Zhang, N.; Tang, Y.; Zhang, H.; Ning, C.; Tian, L.; Li, W.; Zhang, J.; Mao, Y.; Liang, E. Single-electrode triboelectric nanogenerators based on sponge-like porous PTFE thin films for mechanical energy harvesting and self-powered electronics. *J. Mater. Chem. A* **2017**, *5*, 12252–12257. [CrossRef]

59. Gorham, W.F. A New, General Synthetic Method for the Preparation of Linear Poly-p-xylylenes. *J. Polym. Sci.* **1966**, *4*, 3027–3039. [CrossRef]

60. Lo, H.; Tai, Y.-C. Parylene-based electret power generators. *J. Micromechanics Microeng.* **2008**, *18*, 104006. [CrossRef]

61. Genter, S.; Langhof, T.; Paul, O. Electret-based Out-Of-Plane Micro Energy Harvester with Parylene-C Serving as the Electret and Spring Material. *Proc. Eng.* **2015**, *120*, 341–344. [CrossRef]

62. Jeong, G.S.; Baek, D.-H.; Jung, H.C.; Song, J.H.; Moon, J.H.; Hong, S.W.; Kim, I.Y.; Lee, S.-H. Solderable and electroplatable flexible electronic circuit on a porous stretchable elastomer. *Nat. Commun.* **2012**, *3*, 977. [CrossRef] [PubMed]

63. Priya, S. Modeling of electric energy harvesting using piezoelectric windmill. *Appl. Phys. Lett.* **2005**, *87*, 184101. [CrossRef]

64. Zou, H.; Zhang, Y.; Guo, L.; Wang, P.; He, X.; Dai, G.; Zheng, H.; Chen, C.; Wang, A.; Xu, C.; et al. Quantifying the triboelectric series. *Nat. Commun.* **2019**, *10*, 1–9. [CrossRef] [PubMed]

65. Xiong, J.; Cui, P.; Chen, X.; Wang, J.; Parida, K.; Lin, M.-F.; Lee, P.S. Skin-touch-actuated textile-based triboelectric nanogenerator with black phosphorus for durable biomechanical energy harvesting. *Nat. Commun.* **2018**, *9*, 1–9. [CrossRef] [PubMed]

66.　Chen, T.-N.; Wuu, D.-S.; Wu, C.-C.; Chiang, C.-C.; Chen, Y.-P.; Horng, R.-H. Improvements of Permeation Barrier Coatings Using Encapsulated Parylene Interlayers for Flexible Electronic Applications. *Plasma Process. Polym.* **2007**, *4*, 180–185. [CrossRef]

67.　Li, W.; Rodger, D.; Menon, P.; Tai, Y.C. Corrosion Behavior of Parylene-Metal-Parylene Thin Films in Saline. *ECS Trans.* **2008**, *11*, 1. [CrossRef]

68.　Mariello, M.; Guido, F.; Mastronardi, V.M.; Giannuzzi, R.; Algieri, L.; Qualteri, A.; Maffezzoli, A.; De Vittorio, M. Reliability of Protective Coatings for Flexible Piezoelectric Transducers in Aqueous Environments. *Micromachines* **2019**, *10*, 739. [CrossRef]

69.　Mariello, M.; Guido, F.; Mastronardi, V.M.; De Donato, F.; Salbini, M.; Brunetti, V.; Qualtieri, A.; Rizzi, F.; De Vittorio, M. Captive-air-bubble aerophobicity measurements of antibiofouling coatings for underwater MEMS devices. *Nanomater. Nanotechnol.* **2019**, *9*. [CrossRef]